Whole-Body Rocking Motion of a Fusion Peptide in Lipid Bilayers from Size-Dispersed ^{15}N NMR Relaxation

Justin L. Lorieau, John M. Louis, and Ad Bax

Laboratory of Chemical Physics, National Institute of Diabetes and Digestive and Kidney Diseases, National Institutes of Health, Bethesda, MD 20892.

Supporting Information

Materials and Methods

Sample Preparation for NMR. HAfp23 was expressed and purified as previously described.[1] Samples of 0.2-0.4 mM ^{2}H,^{13}C,^{15}N-labeled HAfp23 (GLFGAIAGFI EGGWTGMIDG WYGSGKKKKD) were prepared in ^{2}H-Tris buffer (Cambridge Isotopes) at pH 7.3 and 7% D_2O (Cambridge Isotopes). Underlined residues correspond to the host-peptide,[2] used to facilitate purification. Bicelles were prepared by first dissolving 1,2-di-O-hexyl-sn-glycero-3-phosphatidylcholine (DOHPC; Avanti lipids) in buffer, then adding 1,2-dimyristoyl-sn-glycero-3-phosphocholine (DMPC; Avanti lipids) powder to achieve the desired *q*-ratio (*q*=[DMPC]/[DMPC]). The *q*-ratio of the two components was verified from the integrated intensities of the DMPC and DOHPC methyl signals and from the ^{31}P integrated intensities in fully relaxed one-pulse experiments that included ^{1}H-decoupling. Bicelle samples were prepared with a total wt% ranging from 7.1% to 9.8%. The final pH values of samples used for collecting the relaxation data were pH 7.3 (DPC datasets), pH 7.1 and 7.4 (q=029, 600 MHz and 900 MHz, respectively), pH 7.2 (q=0.52), pH 6.5 (q=0.55) and pH 7.1 (q=0.69). Differences in pH do not impact the structure of the peptide, as judged by NOEs, RDCs[1] and chemical shifts (Figure S1), and they do not impact the relaxation measurements as judged by the close similarity of the R_1 and R_2 rates measured in q=0.52 bicelles (pH 7.2) and q=0.55 bicelles (pH 6.5) in Fig. 2A,B of the main text.

Lipid mixing assay. Lipid mixing was monitored with a fluorescence resonance energy transfer assay:[3] Dioleoylphosphatidylcholine (DOPC), dioleoylphosphatidylethanolamine (DOPE) and cholesterol (Avanti lipids) were mixed in a 1:1:1 ratio in choloroform and dried with a stream of nitrogen gas. Residual chloroform was removed by overnight lyophilyzation. The lipid film was resuspended in 18mM HEPES/MES pH 7.2 by vortexing, followed by a 30 minute resting period at room temperature to hydrate the multilamellar vesicles (MLVs). A total of six freeze-thaw cycles were applied to the resuspension, and the lipids were extruded 15 times through a polycarbonate membrane with 0.1 μm diameter pore size to generate large unilamellar vesicles (LUVs).

LUVs with 0.6 mol% of each of the fluorescent donor and acceptor pairs, N-(7-nitrobenz-2-oxa-1,3-diazol-4-yl)-1,2-dihexadecanoyl-sn-glycero-3-phosphoethanolamine,

triethylammonium salt (NBD-PE; Invitrogen) and (lissamine rhodamine B)-1,2-dihexadecanoyl-sn-glycero-3-phosphoethanolamine, triethylammonium salt (rhodamine DHPE; Invitrogen), respectively, were mixed in a 1:4 ratio to unlabeled LUVs to a final lipid concentration of 3.8 mM in 150 μl. The labeled and unlabeled LUV mixture was equilibrated at 37 °C for 5 minutes before mixing an aliquot of 1 mM peptide in DMSO to a final peptide concentration of 30 μM. Lipid mixing was monitored by the decrease in acceptor fluorescence at 585 nm with a donor excitation wavelength of 465 nm.

NMR Experiments. The ^{15}N relaxation experiments were conducted at 600 MHz and 900 MHz ^{1}H Larmor frequencies, using Bruker Avance III spectrometers. The 600 MHz spectrometer was equipped with a CP-QCI 600 MHz ^{1}H-$^{31}P/^{13}C/^{15}N$-^{2}H cyroprobe including a single-axis gradient coil, and the 900 MHz spectrometer was equipped with a CP-TXI 900 MHz ^{1}H-$^{13}C/^{15}N$-^{2}H cryoprobe, also including a single-axis gradient coil. All experiments were conducted at 305 K.

The ^{15}N relaxation data were collected with R_1, R_2 Heteronuclear Single-Quantum Correlation (HSQC) experiments with either Rance-Kay detection [4] (q=0.29, q=0.52 and q=0.55) or Transverse-Relaxation Optimized Spectroscopy (TROSY) detection (q=0.69).[5] R_2 rates were measured with a $T_{1\rho}$ measurement scheme, using an ^{15}N spin lock field of 1.8 kHz (600 MHz) or 2.0 kHz (900 MHz) and a magnetization-alignment pulse scheme prior to the ^{15}N spin lock period.[6] Spin-lock durations varied between 5 and 95 ms, and T_1 delays varied between 0.1 and 1.8 s. A 3-second recycle delay was used for R_1 and R_2 experiments. In the R_1 experiment, the effect of cross-correlated relaxation was removed by application of band-selective IBURP2 pulses[7] during the longitudinal delay, using special care to ensure that the H_2O magnetization remained in a fully relaxed state for all durations of the relaxation delay. In the R_2 experiment, the effect of cross-correlated relaxation was removed by inverting the amide ^{1}H magnetization midway in the spin-lock period; this was achieved using a composite (90_x-180_y-90_x) pulse immediately followed by a single-lobe sinc flip-back pulse on H_2O to return its magnetization to a relaxed state.[5] A variable-duration ^{15}N temperature compensation pulse was applied to ensure a constant ^{15}N power duty cycle during the entire measurement.[8] The ^{15}N-{^{1}H} NOE experiment[4] was collected with gradient-enhanced

coherence selection,[9] and the NOE spectra with and without ^{1}H saturation were acquired in interleaved mode: the saturation experiment had a 1s delay period before a 4.5s ^{1}H saturation period using a train of 160^o pulses, spaced by 50 ms, and the NONOE reference experiment had a 5.5 s delay period before the start of the pulse sequence.

^{31}P relaxation. An independent measurement of the overall tumbling rate of the bicelles was made on the basis of the DMPC ^{31}P relaxation rates. By measuring ^{31}P transverse relaxation rates, R_2, at two magnetic fields, '*a*' and '*b*', the bicelle τ_R can be readily determined from the difference in R_2 and R_1, provided that the magnitude of the ^{31}P chemical shift anisotropy (CSA), $\langle\Delta\sigma_P\rangle$, is known:[10]

$$2R_2(b) - R_1(b) - 2R_2(a) + R_1(a) \approx \frac{4}{3}\left(c^2(b) - c^2(a)\right)\cdot\tau_R \qquad [S1]$$

where $c^2(x) = (2/15)\ \gamma_P^2\ H_{o,x}^2\ \langle\Delta\sigma_P\rangle^2$, γ_P is the ^{31}P gyromagnetic ratio, and $H_{o,x}$ is the magnetic field strength for measurement '*x*'. Eq S1 isolates τ_R directly from the zero frequency spectral density term, J(0), for a known value of $\langle\Delta\sigma_P\rangle$. For analysis, the standard $\langle\Delta\sigma_P\rangle$ = -45 ppm was used for the L_α phase of DMPC.

^{31}P relaxation data were collected on 500 MHz Avance III and 600 MHz DMX Bruker spectrometers. Both the 500 MHz and 600 MHz spectrometers were equipped with a QXI ^{1}H-^{31}P/^{13}C-^{2}H probe, incl. three-axis gradient coils. The ^{31}P R_1 relaxation rate was measured with a standard phase inversion scheme.[11] The ^{31}P R_2 relaxation rate was derived from an on-resonance R_{1r} experiment, using a 1.0 kHz spin-lock field. A variable-duration ^{31}P temperature compensation pulse was applied to ensure a constant ^{31}P power duty cycle during the entire measurement.[8] Spin-lock durations ranged from 5 to 200 ms, and T_1 delays varied between 0.1 and 1.5 s. Recycle delays of 5 s were used. ^{31}P data and τ_R values derived using eq S1 are presented in Table S5.

Data Analysis. Spectra were processed and analyzed with NMRPipe[12] and Sparky.[13] The ^{15}N R_2 rates were obtained from the measured $R_{1\rho}$ and R_1 rates using the relation $R_2 = (R_{1\rho} - R_1\cos^2\theta)/\sin^2\theta$ where θ is the angle of the spin lock field, $\theta = \arctan(\nu_1/\Omega)$, and ν_1 is the magnitude of the applied RF field and Ω is the chemical shift offset, both in Hz.[14]

Non-linear least-squares fitting of the relaxation data was conducted with MINUIT[15] using a python wrapper. Data modeling, carried out both with the standard Lipari-Szabo formalism[16] and with the extended model-free formalism[17], were used to optimize agreement between predicted and experimental relaxation rates by adjusting the isotropic overall rotational diffusion rate of all phospholipid-HAfp23 complexes, and the internal dynamic parameters which are shared between all micelle and bicelle datasets; these include the residue-specific fast internal motion parameters, τ_f (or τ_i) and $\boldsymbol{S}^2_f$ (or $\boldsymbol{S}^2$), and additionally in the extended Lipari-Szabo analysis, τ_s and $\boldsymbol{S}^2_s$. These latter were optimized together for residues 3-12 and 14-22 (model B), or individually for residues 13 and 23 (model A; see main text). A r_{HN} bond distance of 1.04 Å and $\Delta\sigma$ of -173 ppm were used.[18]

Minima in the relaxation data fits were obtained by conducting a combined grid-search and local minimization over all variables. The search space used was: τ_f = [0, 200 ps], τ_s = [0, 20 ns], $\boldsymbol{S}^2_f$ = [0, 1.0], S^2_s = [0, 1.0]. The overall rotational correlation times were optimized by first searching over a large (~80 ns) window, then refining the search to smaller windows:τ_{R1} = [5, 30 ns], τ_{R2} = [10, 25 ns], τ_{R3} = [20, 38 ns], τ_{R4} = [20, 38 ns] and τ_{R5} = [40, 90 ns] for DPC and the q=0.29, q=0.52, q=0.55 and q=0.69 bicelles, respectively. All grid searches were conducted in 10 steps over each of the specified windows, other than for the order parameters, which were mapped in 5 steps. Each such search was followed by a local minimization using the MIGRAD algorithm, and the global minimum was selected from the local minimum that produced the lowest χ^2.

Experimental errors were estimated from the fit of the data to an exponential relaxation decay curve, and for the heteronuclear NOE experiment from the uncertainty in the relative intensities, with a minimum threshold error of 3% used for all data. Reported errors in the best-fit parameters represent the one standard-deviation confidence region in the χ^2-surface.

Diffusion anisotropy. Rotational diffusion anisotropy of oblate spheroids, expressed as the ratio of the rotational diffusion constants parallel and perpendicular to the unique axis, $D_{//}/D_{\perp}$ has a limiting value > 0.8 for oblate spheroids. Due to the very limited distribution in orientations, with all N-H vectors roughly orthogonal to the bicelle normal,

no experimental determination of diffusion anisotropy of HAfp23 is feasible. However, the maximum deviation of the motional correlation time for any given vector from the effective rotational correlation time, given by $1/(4\ D_{\perp}+2D_{//})$, is only 7.7%. The approximately parallel orientation of N-H vectors for residues 3-12 and 14-23 makes the issue of diffusion anisotropy irrelevant for these amides, but could possibly have a small impact on the motional parameters for G13, whose orientation relative to the bilayer normal has greater uncertainty. If G13 were assigned a global rotational correlation time 7% longer than the value best-fitted for the other residues, this decreases its best-fitted $\boldsymbol{S}^2_s$ by 0.02 and increases its τ_s by 0.1 ns, which is within the reported error.

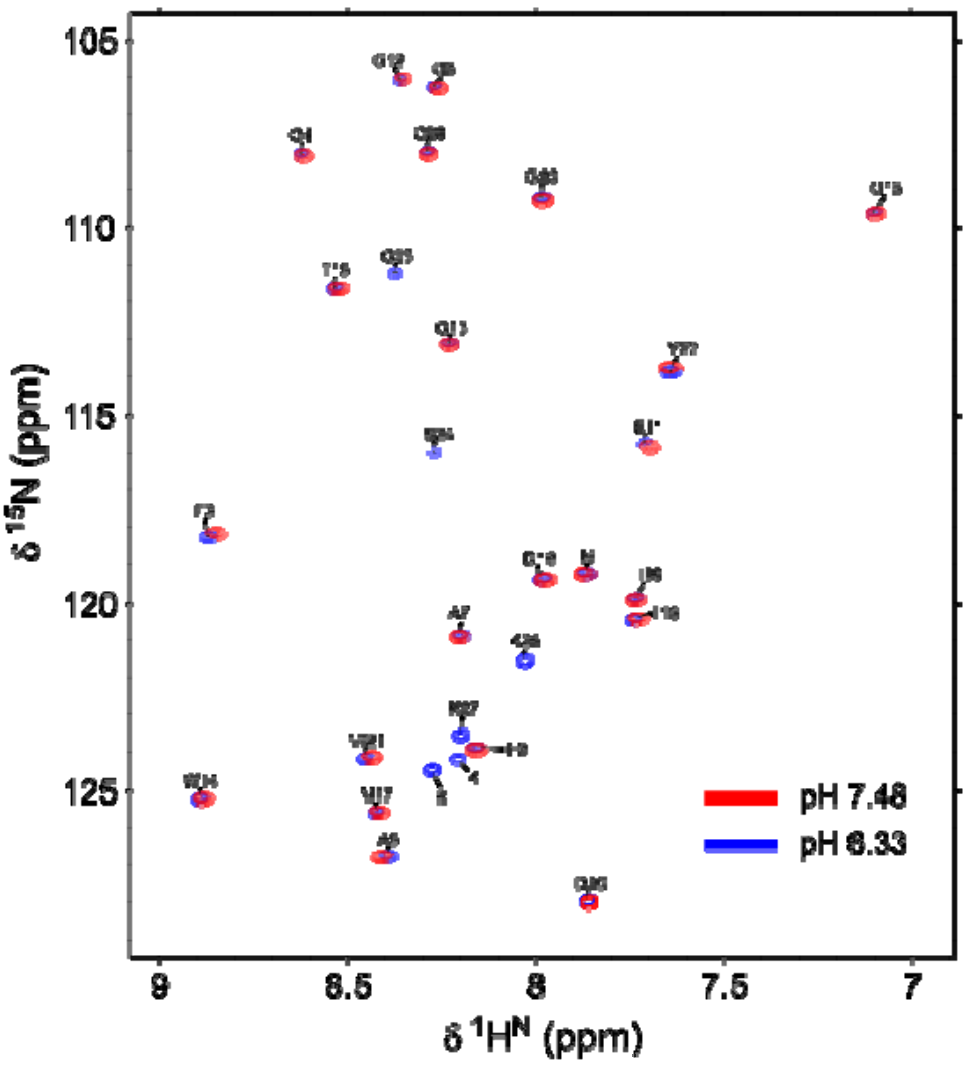

Figure S1. Superimposed ^{1}H-^{15}N TROSY-HSQC spectra of 0.3 mM ^{2}H,^{13}C,^{15}N-labeled HAfp23 in q=0.55 bicelles (9.5% w/v), recorded at pH 7.48 and 6.33. Additional residues in the disordered C-terminal solubilization tag (residues 24-30) can be seen at the lower pH due to a decrease in the hydrogen exchange rate by a factor of ~14.

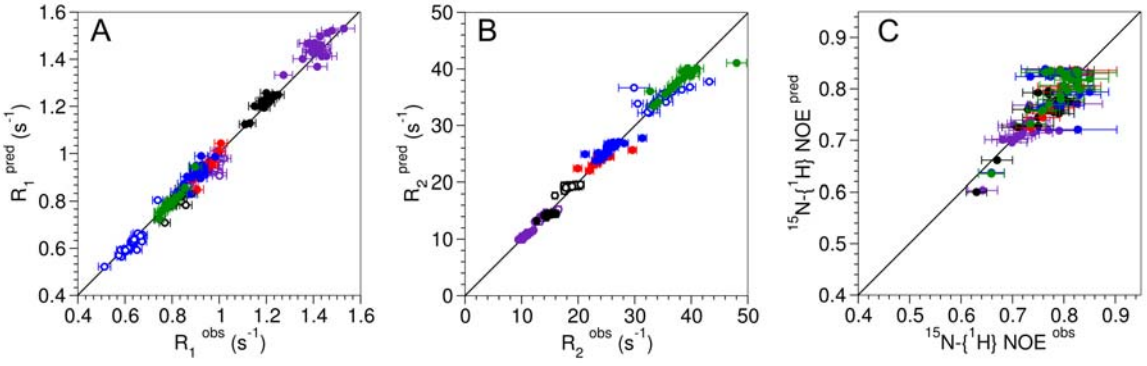

Figure S2. Correlations between experimental relaxation rates and results from residue-specific fits of the ^{15}N relaxation data, carried out independently for the DPC micelle and each bicelle size using the standard Lipari-Szabo formalism.[16] Data are shown for HAfp23 dissolved in DPC micelles (purple) and bicelles of three sizes: small (q=0.29, black), medium (q=0.52, red, and q=0.55, blue) and large (q=0.69, green). Relaxation rates were measured at 600 MHz (filled circles) and 900 MHz (open circles). Because collection of high S/N ^{15}N-{^{1}H}NOE data at q=0.69 is not feasible within a reasonable amount of measurement time, and considering that far into the slow motion limit the ^{15}N-{^{1}H}NOE is independent of τ_c, data from the q=0.52 dataset were used to fit this relaxation data. The best-fitted overall rotational correlation times were 8.2 ± 0.1 ns (DPC); 11.1 ± 0.1 ns (q=0.29), 21.0 ± 0.3 ns (q=0.52), 23.3 ± 0.2 ns (q=0.55) and 35.9 ± 0.6 ns (q=0.69). The F3-E11 and G13-Y22 $\boldsymbol{S}^2$ values are greater than ~0.9 for DPC and q=0.29 bicelles, and between 0.6 and 0.9 for the larger bicelle sizes (Table S2).

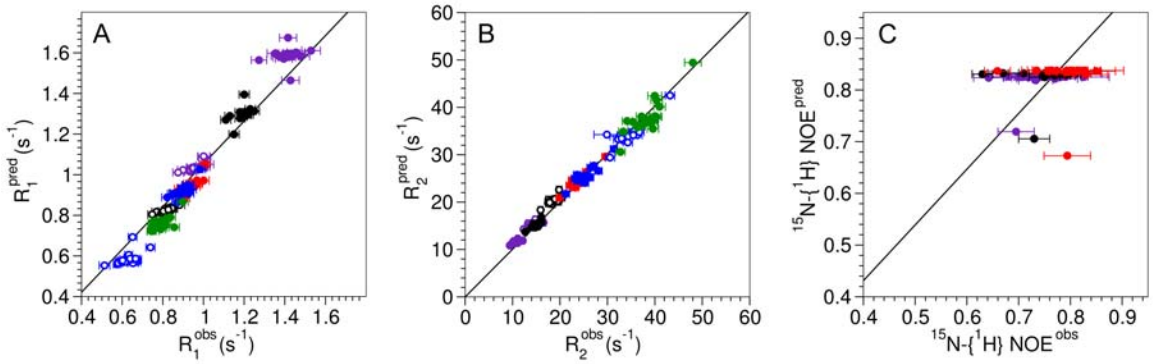

Figure S3. Correlations between experimental relaxation rates and results from residue-specific fits of the ^{15}N relaxation data, carried out using a model A fit but with the standard Lipari-Szabo formalism.[16] Data are shown for HAfp23 dissolved in DPC micelles (purple) and bicelles of three sizes: small (q=0.29, black), medium (q=0.52, red, and q=0.55, blue) and large (q=0.69, green). Relaxation rates were measured at 600 MHz (filled circles) and 900 MHz (open circles). The best-fitted overall rotational correlation times were 10.5 ns (DPC); 14.8 ns (q=0.29), 26.9 ns (q=0.52), 28.4 ns (q=0.55) and 45.6 ns (q=0.69).

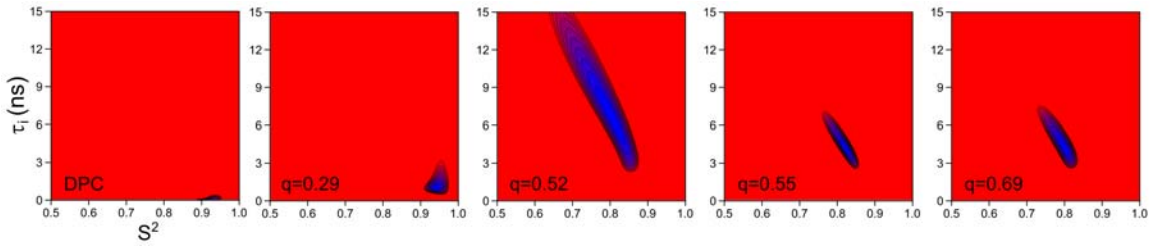

Figure S4. Contour plots of χ^2 as a function of the internal dynamic parameters, S^2 and τ_i, for the standard Lipari-Szabo fits to the individual datasets collected for HAfp23 solubilized in DPC and bicelles of different size. Shown are the contour plots for the internal motional parameters, τ_i and S^2, at the 95% confidence interval for residue Gly16, which is representative for residues F3-Y22.

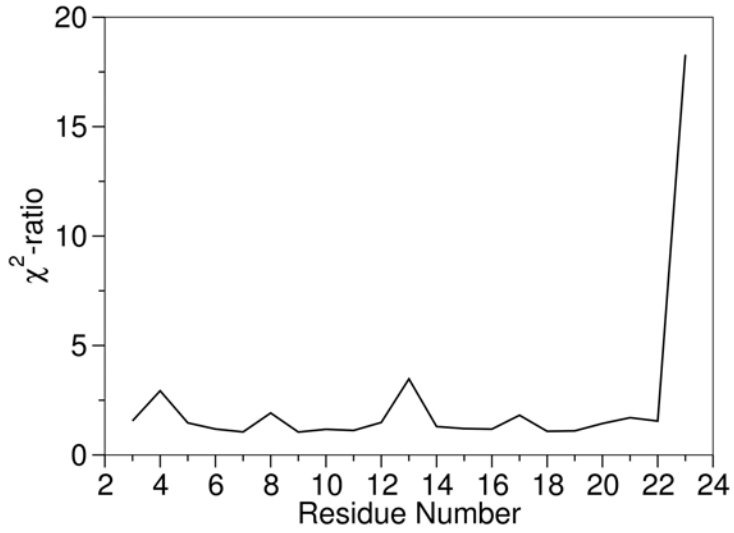

Figure S5. Plot of the χ^2-ratio between model A and model B fits as a function of residue number (see main text for a description of these fits). In both cases, there are a total of 399 relaxation data points. In model B, there are two free parameters (τ_f, $\boldsymbol{S}^2_f$) for each of the 21 residues, and seven global free parameters (τ_s, $\boldsymbol{S}^2_s$, and five overall rotational correlation times).

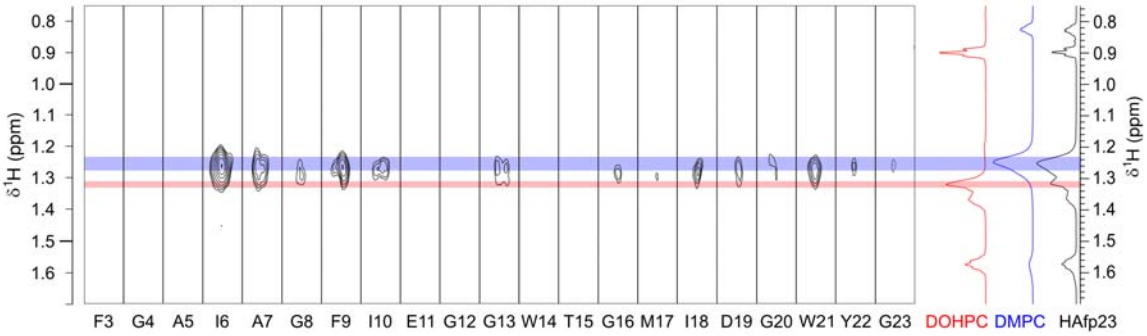

Figure S6. $^{1}H^{N}$-^{1}H strip-plots taken from a 3D ^{15}N NOESY-HMQC spectrum (200 ms NOE mixing time, collected at 600 MHz) showing intermolecular NOEs from the DMPC methylene protons of the bicelles (blue shading) to backbone amides in ^{2}H,^{13}C,^{15}N-labeled HAfp23 (q=0.61, 9.8% w/v). On the right margin the 1D ^{1}H spectra are shown for the HAfp23 sample on which the NOE data were recorded (black), and spectra for q=0.61 bicelles consisting of protonated DOHPC and deuterated DMPC (red), and for protonated DMPC and deuterated DHPC (blue; perdeuterated DOHPC is not commercially available). The off-center correlation to the DMPC methylene protons observed for G13 is due to partial overlap with the A7 peak in both the $^{1}H^{N}$ and ^{15}N dimensions.

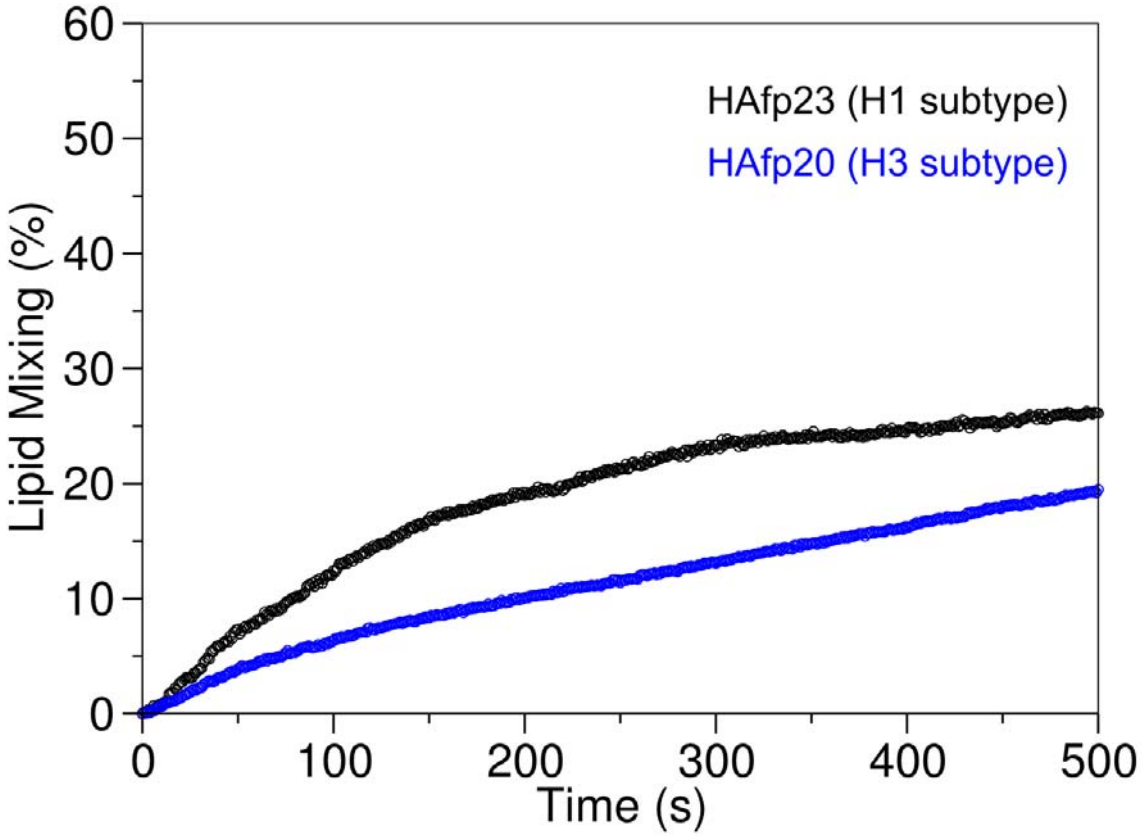

Figure S7. Lipid mixing induced by the hemagglutinin fusion peptides HAfp20 H3-subtype (blue trace) and HAfp23 H1-subtype (black trace). The fluorescence scale has been calibrated such that the zero level corresponds to the initial residual fluorescence of the labeled vesicles and the 100% value to complete mixing of all of the lipids in the system (obtained by adding reduced Triton X-100 to a final concentration of 50 mM).

Table S1-A. ^{15}N Backbone relaxation data for HAfp23 in DPC at 600 and 900 MHz (data from reference [1])

Spin	R_2 /600 (s^{-1})		R_1 /600 (s^{-1})		NOE /600		R_2 /900 (s^{-1})		R_1 /600 (s^{-1})	
F3	10.0	± 0.3	1.46	± 0.04	0.79	± 0.04	13.2	± 0.4	1.00	± 0.03
G4	11.0	± 0.3	1.53	± 0.05	0.83	± 0.05	14.3	± 0.4	0.99	± 0.03
A5	11.8	± 0.4	1.46	± 0.04	0.73	± 0.03	15.7	± 0.5	1.02	± 0.03
I6	10.7	± 0.3	1.44	± 0.04	0.73	± 0.04	13.8	± 0.4	0.90	± 0.03
A7	10.8	± 0.3	1.42	± 0.04	0.71	± 0.03	14.2	± 0.4	0.97	± 0.03
G8	11.0	± 0.3	1.40	± 0.04	0.77	± 0.04	14.1	± 0.4	0.94	± 0.03
F9	11.2	± 0.3	1.37	± 0.04	0.68	± 0.04	14.8	± 0.4	0.97	± 0.03
I10	10.8	± 0.3	1.41	± 0.04	0.71	± 0.04	13.9	± 0.4	0.94	± 0.03
E11	11.2	± 0.3	1.38	± 0.04	0.70	± 0.03	15.5	± 0.5	0.94	± 0.03
G12	10.2	± 0.3	1.27	± 0.04	0.71	± 0.04	13.3	± 0.4	0.88	± 0.03
G13	11.1	± 0.3	1.43	± 0.04	0.70	± 0.04	14.8	± 0.4	1.01	± 0.03
W14	10.5	± 0.3	1.41	± 0.04	0.77	± 0.05	13.6	± 0.4	0.98	± 0.03
T15	10.5	± 0.3	1.35	± 0.04	0.70	± 0.03	13.6	± 0.4	0.94	± 0.03
G16	10.9	± 0.3	1.40	± 0.04	0.72	± 0.03	13.8	± 0.4	0.97	± 0.03
M17	12.1	± 0.4	1.48	± 0.04	0.77	± 0.04	16.5	± 0.5	0.99	± 0.03
I18	10.8	± 0.3	1.43	± 0.04	0.78	± 0.04	13.9	± 0.4	0.95	± 0.03
D19	10.7	± 0.3	1.41	± 0.04	0.72	± 0.03	14.2	± 0.4	0.95	± 0.03
G20	10.5	± 0.3	1.43	± 0.04	0.74	± 0.04	13.8	± 0.4	0.99	± 0.03
W21	11.3	± 0.3	1.41	± 0.04	0.73	± 0.04	14.3	± 0.4	0.99	± 0.03
Y22	11.1	± 0.3	1.43	± 0.04	0.74	± 0.04	14.3	± 0.4	0.95	± 0.03
G23	9.4	± 0.3	1.42	± 0.04	0.64	± 0.03	12.3	± 0.4	1.00	± 0.03

Table S1-B. ^{15}N Backbone relaxation data for HAfp23 in q=0.29 bicelles at 600 and 900 MHz

Spin	R_2 /600 (s^{-1})		R_1 /600 (s^{-1})		NOE /600		R_2 /900 (s^{-1})		R_1 /600 (s^{-1})	
3	14.0	± 0.4	1.23	± 0.03	0.79	± 0.03	17.5	± 0.5	0.84	± 0.03
4	14.6	± 0.4	1.23	± 0.03	0.79	± 0.04	18.4	± 0.6	0.84	± 0.03
5	16.1	± 0.4	1.25	± 0.03	0.75	± 0.03	20.2	± 0.6	0.88	± 0.03
6	14.6	± 0.4	1.13	± 0.03	0.83	± 0.03	17.7	± 0.5	0.77	± 0.02
7	14.9	± 0.4	1.19	± 0.03	0.80	± 0.03	18.6	± 0.6	0.82	± 0.03
8	14.9	± 0.4	1.18	± 0.03	0.75	± 0.03	18.7	± 0.6	0.79	± 0.02
9	15.5	± 0.4	1.21	± 0.03	0.77	± 0.03	19.7	± 0.6	0.82	± 0.02
10	14.5	± 0.4	1.19	± 0.03	0.79	± 0.03	18.1	± 0.5	0.80	± 0.02
11	15.0	± 0.4	1.19	± 0.03	0.71	± 0.03	19.5	± 0.6	0.80	± 0.02
12	14.4	± 0.4	1.11	± 0.03	0.67	± 0.03	17.6	± 0.5	0.75	± 0.02
13	16.1	± 0.4	1.15	± 0.03	0.73	± 0.03	19.8	± 0.6	0.86	± 0.03
14	14.3	± 0.4	1.22	± 0.03	0.78	± 0.03	18.0	± 0.5	0.85	± 0.03
15	15.2	± 0.4	1.18	± 0.03	0.81	± 0.03	17.5	± 0.5	0.82	± 0.03
16	14.6	± 0.4	1.19	± 0.03	0.78	± 0.03	18.3	± 0.6	0.84	± 0.03
17	15.5	± 0.4	1.21	± 0.03	0.77	± 0.03	20.4	± 0.6	0.84	± 0.03
18	14.6	± 0.4	1.22	± 0.03	0.79	± 0.03	18.0	± 0.5	0.82	± 0.03
19	14.6	± 0.4	1.21	± 0.03	0.77	± 0.03	18.4	± 0.6	0.80	± 0.02
20	15.0	± 0.4	1.20	± 0.03	0.77	± 0.03	18.1	± 0.5	0.84	± 0.03
21	14.6	± 0.4	1.22	± 0.03	0.79	± 0.03	19.0	± 0.6	0.85	± 0.03
22	14.6	± 0.4	1.19	± 0.03	0.75	± 0.03	17.8	± 0.5	0.83	± 0.03
23	12.7	± 0.4	1.20	± 0.03	0.63	± 0.02	15.9	± 0.5	0.89	± 0.03

Table S1-C. ^{15}N Backbone relaxation data for HAfp23 in q=0.52 bicelles recorded at 600 MHz

Spin	R_2 (s^{-1})		R_1 (s^{-1})		NOE	
F3	23.2	± 0.8	0.97	± 0.03	0.80	± 0.05
G4	23.2	± 0.8	1.00	± 0.03	0.77	± 0.05
A5	25.5	± 0.8	0.97	± 0.03	0.83	± 0.04
I6	23.1	± 0.8	0.90	± 0.03	0.79	± 0.03
A7	24.1	± 0.8	0.96	± 0.03	0.77	± 0.04
G8	23.5	± 0.8	0.91	± 0.03	0.76	± 0.03
F9	23.2	± 0.8	0.92	± 0.03	0.81	± 0.03
I10	23.5	± 0.8	0.90	± 0.03	0.74	± 0.03
E11	24.0	± 0.8	0.88	± 0.03	0.83	± 0.08
G12	22.5	± 0.8	0.89	± 0.03	0.76	± 0.05
G13	29.6	± 0.8	0.91	± 0.03	0.79	± 0.05
W14	23.7	± 0.8	0.96	± 0.03	0.76	± 0.03
T15	22.0	± 0.8	0.96	± 0.03	0.83	± 0.03
G16	24.0	± 0.8	0.94	± 0.03	0.83	± 0.03
M17	25.6	± 0.8	0.97	± 0.03	0.81	± 0.03
I18	23.9	± 0.8	0.93	± 0.03	0.83	± 0.03
D19	23.4	± 0.8	0.92	± 0.03	0.80	± 0.03
G20	24.0	± 0.8	0.93	± 0.03	0.85	± 0.04
W21	24.6	± 0.8	0.94	± 0.03	0.79	± 0.03
Y22	23.4	± 0.8	0.94	± 0.03	0.80	± 0.03
G23	19.9	± 0.8	1.01	± 0.03	0.66	± 0.03

Table S1-D. ^{15}N Backbone relaxation data for HAfp23 in q=0.55 bicelles recorded at 600 and 900 MHz

Spin	R_2 /600 (s^{-1})		R_1 /600 (s^{-1})		R_2 /900 (s^{-1})		R_1 /900 (s^{-1})	
F3	25.1	± 0.8	0.92	± 0.03	33	± 1	0.62	± 0.03
G4	25.3	± 0.8	0.93	± 0.03	34	± 1	0.63	± 0.02
A5	27.1	± 0.8	0.92	± 0.03	40	± 1	0.63	± 0.02
I6	24.3	± 0.8	0.86	± 0.03	33	± 1	0.59	± 0.02
A7	25.7	± 0.8	0.90	± 0.03	36	± 1	0.59	± 0.02
G8	25.2	± 0.8	0.88	± 0.03	35	± 1	0.57	± 0.02
F9	23.2	± 0.8	0.92	± 0.03	33	± 2	0.67	± 0.02
I10	26.4	± 0.8	0.93	± 0.03	35	± 1	0.58	± 0.02
E11	26.1	± 0.8	0.85	± 0.03	30	± 3	0.65	± 0.03
G12	23.6	± 0.8	0.82	± 0.03	36	± 1	0.51	± 0.03
G13	31.4	± 0.8	0.87	± 0.03	43	± 1	0.65	± 0.02
W14	25.4	± 0.8	0.91	± 0.03	36	± 1	0.65	± 0.02
T15	23.7	± 0.8	0.90	± 0.03	32	± 1	0.61	± 0.02
G16	25.7	± 0.8	0.92	± 0.03	37	± 1	0.64	± 0.02
M17	26.4	± 0.8	0.94	± 0.03	38	± 1	0.64	± 0.02
I18	25.7	± 0.8	0.92	± 0.03	35	± 1	0.60	± 0.02
D19	25.2	± 0.8	0.90	± 0.03	34	± 1	0.61	± 0.02
G20	25.3	± 0.8	0.90	± 0.03	35	± 1	0.68	± 0.02
W21	28.1	± 0.8	0.92	± 0.03	37	± 1	0.67	± 0.02
Y22	24.1	± 0.8	0.93	± 0.03	33	± 1	0.60	± 0.02
G23	21.3	± 0.8	0.98	± 0.03	31	± 1	0.74	± 0.02

Table S1-E. ^{15}N Backbone relaxation data for HAfp[23] in q=0.69 bicelles at 600 MHz

Spin	R_2 (s^{-1})		R_1 (s^{-1})	
F3	39.6	± 1.2	0.77	± 0.02
G4	33.3	± 1.0	0.82	± 0.02
A5	40.0	± 1.5	0.84	± 0.03
I6	35.4	± 1.1	0.75	± 0.02
A7	40.3	± 1.2	0.81	± 0.02
G8	39.1	± 1.2	0.79	± 0.02
F9	39.2	± 1.4	0.76	± 0.02
I10	38.6	± 1.2	0.79	± 0.02
E11	34.2	± 1.0	0.86	± 0.03
G12	37.2	± 1.1	0.75	± 0.03
G13	48.0	± 1.8	0.74	± 0.02
W14	39.3	± 1.2	0.77	± 0.02
T15	36.4	± 1.1	0.75	± 0.02
G16	40.0	± 1.2	0.81	± 0.02
M17	40.4	± 1.2	0.79	± 0.02
I18	39.3	± 1.2	0.78	± 0.02
D19	37.8	± 1.1	0.78	± 0.02
G20	38.6	± 1.2	0.80	± 0.02
W21	41.0	± 1.2	0.78	± 0.02
Y22	36.9	± 1.1	0.79	± 0.02
G23	32.8	± 1.0	0.90	± 0.03

Table S2. Individual Lipari-Szabo fits of the relaxation data measured in the presence of DPC micelles and different size bicelles.[a,b]

Spin	τ_i (ns) DPC	S^2 DPC	τ_i (ns) q=0.29	S^2 q=0.29	τ_i (ns) q=0.52	S^2 q=0.52	τ_i (ns) q=0.55	S^2 q=0.55	τ_i (ns) q=0.69	S^2 q=0.69
F3	[0.05,0.11]	[0.89,0.92]	[1,1.5]	[0.91,0.94]	[4.9,11.2]	[0.69,0.82]	[6.7,10.5]	[0.68,0.77]	[2.5,6.4]	[0.78,0.85]
G4	[0.45,1.3]	[0.94,0.97]	[0.9,1.7]	[0.92,0.95]	[1.7,3.7]	[0.81,0.83]	[5,7.8]	[0.73,0.8]	[9.5,12.7]	[0.57,0.64]
A5	[0.12,0.73]	[0.96,0.98]	[1.2,2.2]	[0.93,0.95]	[2.6,5.2]	[0.82,0.86]	[2.6,3.7]	[0.84,0.86]	[3,5.2]	[0.77,0.81]
I6	[0.05,0.1]	[0.89,0.92]	[0,0.1]	[0.94,0.96]	[1.9,15]	[0.62,0.79]	[10.1,14.6]	[0.62,0.72]	[9.2,13]	[0.62,0.71]
A7	[0.08,0.18]	[0.91,0.94]	[0.8,1.6]	[0.94,0.97]	[1.9,3.4]	[0.83,0.86]	[4.9,7.9]	[0.76,0.83]	[2.3,3.8]	[0.8,0.82]
G8	[0.02,0.09]	[0.91,0.94]	[0.5,0.9]	[0.94,0.96]	[1.8,2.6]	[0.85,0.87]	[6.3,9.8]	[0.73,0.81]	[2.2,3.5]	[0.81,0.83]
F9	[0.1,0.23]	[0.92,0.95]	[0.8,1.7]	[0.95,0.97]	[7.3,15]	[0.65,0.8]	[7.4,11.4]	[0.61,0.71]	[3.3,7.3]	[0.76,0.84]
I10	[0.07,0.14]	[0.9,0.93]	[0.7,1.2]	[0.94,0.96]	[1.7,2.2]	[0.85,0.87]	[4.7,7.5]	[0.77,0.83]	[2.1,2.8]	[0.81,0.83]
E11	[0.08,0.2]	[0.93,0.96]	[0.4,0.8]	[0.94,0.96]	[6,14.7]	[0.71,0.85]	[1.5,2.5]	[0.85,0.86]	[7.4,10.2]	[0.61,0.68]
G12	[0.03,0.06]	[0.84,0.87]	[0.1,0.1]	[0.9,0.92]	[5.5,15]	[0.66,0.71]	[13.4,15]	[0.66,0.7]	[6.4,10.2]	[0.69,0.77]
G13	[0.11,0.58]	[0.93,0.96]	[0.6,1]	[0.95,0.97]	[2.4,4.1]	[0.89,0.91]	[2.1,2.7]	[0.87,0.89]	[2.4,3.8]	[0.84,0.86]
W14	[0.05,0.13]	[0.9,0.93]	[1,1.5]	[0.92,0.94]	[2,2.8]	[0.83,0.85]	[2.1,3.2]	[0.83,0.85]	[2.2,3.2]	[0.82,0.84]
T15	[0.06,0.11]	[0.88,0.91]	[0.9,1.5]	[0.94,0.96]	[2.8,15]	[0.55,0.72]	[10,13.9]	[0.6,0.69]	[7.9,11.6]	[0.66,0.74]
G16	[0.07,0.15]	[0.91,0.94]	[0.8,1.3]	[0.93,0.95]	[3.5,9.7]	[0.75,0.86]	[3.2,5.2]	[0.8,0.84]	[3.2,5.4]	[0.78,0.82]
M17	[0,9.74]	[0.98,1]	[0.9,1.9]	[0.95,0.97]	[2.5,4.7]	[0.83,0.86]	[2.8,4.1]	[0.82,0.85]	[2.8,5]	[0.8,0.83]
I18	[0.03,0.09]	[0.91,0.94]	[0.9,1.5]	[0.93,0.95]	[4.1,10.6]	[0.74,0.85]	[5.3,7.9]	[0.75,0.81]	[3.7,6.6]	[0.76,0.82]
D19	[0.07,0.13]	[0.9,0.93]	[0.7,1.2]	[0.94,0.96]	[6,14]	[0.68,0.83]	[5.6,8.6]	[0.73,0.8]	[4.7,8.1]	[0.72,0.8]
G20	[0.07,0.15]	[0.9,0.93]	[0.8,1.3]	[0.93,0.95]	[4.6,10.9]	[0.74,0.85]	[2.6,4.5]	[0.8,0.84]	[4.3,7.2]	[0.74,0.8]
W21	[0.07,0.21]	[0.93,0.96]	[1,1.8]	[0.93,0.95]	[2,4.5]	[0.84,0.87]	[2.3,3.2]	[0.84,0.85]	[2.6,4.3]	[0.81,0.84]
Y22	[0.06,0.17]	[0.92,0.95]	[0.7,1.1]	[0.92,0.94]	[4.7,11.8]	[0.7,0.84]	[8.6,12.4]	[0.64,0.72]	[5.9,9.1]	[0.69,0.77]
G23	[0.09,0.13]	[0.84,0.86]	[0.8,0.9]	[0.85,0.87]	[1.5,1.8]	[0.76,0.79]	[1.5,1.8]	[0.77,0.79]	[1.8,2]	[0.73,0.75]

(a) The best-fit overall rotational correlation times are 8.2 ± 0.1 ns (DPC), 11.1 ± 0.1 ns (q=0.29), 21.0 ± 0.5 ns (q=0.52), 23.3 ± 0.8 ns (q=0.55) and 35.9 ± 0.6 ns (q=0.69). The search space for the overall and internal motional parameters match those of the combined fit (see Data Analysis) except τ_i, which was fit over the range of 0-15 ns, and τ_R, which was fit over the range 5-15 ns (DPC), 10-25 ns (q=0.29), 15-35 ns (q=0.52 and q=0.55) and 30-50 ns (q=0.69). For fits without a heteronuclear NOE measurement (q=0.55 and q=0.69), the q=0.52 NOE dataset was used in the fits. (b) Reported ranges represent the one standard-deviation confidence region on the χ^2-surface.

Table S3. ^{15}N backbone dynamic parameters for HAfp[23] in DPC micelles and bicelles using the model A fit.[a,b]

Residue	τ_f (ps)	S^2_f	τ_s (ns)	S^2_s	χ^2
F3	[0,12]	[0.86,0.87]	[3.6,5.3]	[0.68,0.72]	22.3
G4	[7,43]	[0.91,0.94]	[7.2,9.8]	[0.56,0.63]	15.5
A5	[11,57]	[0.93,0.95]	[4,5.6]	[0.71,0.75]	17.1
I6	[2,16]	[0.85,0.87]	[5.4,7.7]	[0.64,0.7]	16.9
A7	[9,29]	[0.88,0.9]	[4.4,5.9]	[0.7,0.73]	15.8
G8	[14,32]	[0.87,0.89]	[5,6.8]	[0.68,0.73]	7.6
F9	[2,24]	[0.87,0.89]	[3.4,5.1]	[0.71,0.75]	45.7
I10	[16,34]	[0.87,0.89]	[4.9,6.5]	[0.68,0.72]	14.6
E11	[41,83]	[0.88,0.92]	[6.2,10.1]	[0.61,0.7]	50.5
G12	[21,35]	[0.81,0.83]	[4.6,6.4]	[0.7,0.74]	25.5
G13	[0,49]	[0.94,0.96]	[2.1,2.7]	[0.8,0.81]	55.1
W14	[0,17]	[0.86,0.88]	[3.3,4.3]	[0.72,0.74]	12.9
T15	[3,19]	[0.85,0.87]	[4.6,6.6]	[0.66,0.71]	36.0
G16	[0,25]	[0.87,0.89]	[3.4,4.4]	[0.72,0.74]	13.7
M17	[1,43]	[0.93,0.95]	[4.3,6.5]	[0.7,0.75]	15.1
I18	[0,174]	[0.88,0.9]	[4.6,6]	[0.68,0.72]	11.4
D19	[9,25]	[0.87,0.89]	[4.6,6.3]	[0.68,0.72]	8.9
G20	[0,8]	[0.87,0.88]	[3.2,4]	[0.72,0.74]	16.6
W21	[0,124]	[0.89,0.9]	[3.1,3.8]	[0.74,0.76]	10.8
Y22	[10,30]	[0.87,0.9]	[5.5,7.8]	[0.63,0.69]	13.7
G23	[29,41]	[0.79,0.81]	[3.2,4]	[0.66,0.68]	9.1

(a) The overall rotational correlation times were set to the optimal values from the model B fit: τ_R = 10.9 ns (DPC), τ_R = 15.1 ns (q=0.29 bicelles), τ_R = 26.6 ns (q=0.52), τ_R = 29.0 ns (q=0.55), and τ_R = 44.2 ns (q=0.69).

(b) Reported ranges represent the one standard-deviation confidence region on the χ^2-surface.

Table S4. ^{15}N Backbone dynamics parameters for HAfp[23] in DPC micelles and bicelles.[a,b]

Spin	Model	τ_f (ps)	S^2_f	τ_s (ns) [(a)]	S^2_s [(a)]	χ^2
F3	B	[11,27]	[0.86,0.88]	[4.5,5.7]	[0.68,0.73]	36.3
G4	B	[18,36]	[0.88,0.89]	[4.5,5.7]	[0.68,0.73]	44.1
A5	B	[0,32]	[0.93,0.95]	[4.5,5.7]	[0.68,0.73]	25.0
I6	B	[0,9]	[0.84,0.85]	[4.5,5.7]	[0.68,0.73]	18.7
A7	B	[8,24]	[0.88,0.89]	[4.5,5.7]	[0.68,0.73]	16.6
G8	B	[4,18]	[0.86,0.88]	[4.5,5.7]	[0.68,0.73]	13.3
F9	B	[11,27]	[0.88,0.89]	[4.5,5.7]	[0.68,0.73]	45.4
I10	B	[12,24]	[0.86,0.88]	[4.5,5.7]	[0.68,0.73]	16.7
E11	B	[24,40]	[0.86,0.88]	[4.5,5.7]	[0.68,0.73]	55.0
G12	B	[14,24]	[0.81,0.83]	[4.5,5.7]	[0.68,0.73]	37.1
G13	A	[0,49]	[0.94,0.96]	[2.1,2.7]	[0.8,0.81]	55.1
W14	B	[15,29]	[0.87,0.89]	[4.5,5.7]	[0.68,0.73]	18.8
T15	B	[8,20]	[0.85,0.86]	[4.5,5.7]	[0.68,0.73]	42.0
G16	B	[5,21]	[0.88,0.90]	[4.5,5.7]	[0.68,0.73]	18.1
M17	B	[0,29]	[0.92,0.94]	[4.5,5.7]	[0.68,0.73]	25.4
I18	B	[0,18]	[0.88,0.89]	[4.5,5.7]	[0.68,0.73]	12.6
D19	B	[9,21]	[0.87,0.88]	[4.5,5.7]	[0.68,0.73]	9.3
G20	B	[7,23]	[0.88,0.89]	[4.5,5.7]	[0.68,0.73]	26.1
W21	B	[4,24]	[0.90,0.91]	[4.5,5.7]	[0.68,0.73]	20.6
Y22	B	[11,23]	[0.86,0.88]	[4.5,5.7]	[0.68,0.73]	19.3
G23	A	[29,41]	[0.79,0.81]	[3.2,4.0]	[0.66,0.68]	9.1

(a) The τ_s and S^2_s for model B spins represent the globally-fitted value over all model B spins. The best-fit overall rotational correlation times τ_R = 10.9 ± 0.1 ns (DPC), τ_R = 15.1 ± 0.2 ns (q=0.29 bicelles), τ_R = 26.6 ± 0.4 ns (q=0.52), τ_R = 29.0 ± 0.4 ns (q=0.55), and τ_R = 44.2 ± 0.7 ns (q=0.69) were used for all model model B fits. Entries for G13 and G23 are those from Table S3.

(b) Reported ranges represent the one standard-deviation confidence region on the χ^2-surface.

Table S5. Bicelle rotational correlation times in the presence of HAfp23 derived from ^{31}P relaxation

Bicelle Formulation [(a)]	R_2 (s^{-1}) [(b)]	R_1 (s^{-1}) [(b)]	R_2 (s^{-1}) [(c)]	R_1 (s^{-1}) [(c)]	τ_R (ns)
small + HAfp23	5.6 ± 0.1	1.02 ± 0.01	7.8 ± 0.1	1.28 ± 0.02	15 ± 2
medium + HAfp23	11.0 ± 0.1	1.09 ± 0.01	15.1 ± 0.2	1.34 ± 0.02	31 ± 3
large + HAfp23	14.5 ± 0.2	1.10 ± 0.02	20.0 ± 0.3	1.36 ± 0.02	42 ± 4

(a) The lipid-to-solvent %w/v and q-ratio for the different bicelle sizes are: small, 7.2% and q=0.29; medium, 9.0% and q=0.55; large, 9.8% and q=0.69. The peptide-to-bicelle ratios are 0.5 (small), 0.4 (medium) and 0.9 (large). The bicelle q-ratio is derived from the relative integrals of the DMPC to DOHPC ^{31}P signal intensities, recorded under fully relaxed conditions and 1-kHz ^{1}H decoupling.

(b) 202.5 MHz ^{31}P frequency (500 MHz ^{1}H)

(c) 242.9 MHz ^{31}P frequency (600 MHz ^{1}H)

References

(1) Lorieau, J. L.; Louis, J. M.; Bax, A. *Proc. Natl. Acad. Sci. U. S. A.* **2010**, *107*, 11341-11346.
(2) Han, X.; Tamm, L. K. *Proc. Natl. Acad. Sci. U. S. A.* **2000**, *97*, 13097-13102.
(3) Jaroniec, C. P.; Kaufman, J. D.; Stahl, S. J.; Viard, M.; Blumenthal, R.; Wingfield, P. T.; Bax, A. *Biochemistry* **2005**, *44*, 16167-16180.
(4) Farrow, N. A.; Muhandiram, R.; Singer, A. U.; Pascal, S. M.; Kay, C. M.; Gish, G.; Shoelson, S. E.; Pawson, T.; Forman-Kay, J. D.; Kay, L. E. *Biochemistry* **1994**, *33*, 5984-6003.
(5) Chill, J. H.; Louis, J. M.; Baber, J. L.; Bax, A. *J. Biomol. NMR* **2006**, *36*, 123-136.
(6) Hansen, D. F.; Kay, L. E. *J. Biomol. NMR* **2007**, *37*, 245-255.
(7) Geen, H.; Freeman, R. *J. Magn. Reson.* **1991**, *93*, 93-141.
(8) Wang, A. C.; Bax, A. *J. Biomol. NMR* **1993**, *3*, 715-720.
(9) Kay, L. E.; Keifer, P.; Saarinen, T. *J. Am. Chem. Soc.* **1992**, *114*, 10663-10665.
(10) Kay, L. E.; Torchia, D. A.; Bax, A. *Biochemistry* **1989**, *28*, 8972-8979; Fushman, D.; Tjandra, N.; Cowburn, D. *J. Am. Chem.Soc.* **1999**, *121*, 8577-8582.
(11) Torchia, D. A. *J. Magn. Reson.* **1978**, *30*, 613-616.
(12) Delaglio, F.; Grzesiek, S.; Vuister, G. W.; Zhu, G.; Pfeifer, J.; Bax, A. *J. Biomol. NMR* **1995**, *6*, 277-293.
(13) Goddard, T. D.; Kneller, D. G. University of California, San Francisco.
(14) Cavanagh, J.; Fairbrother, W. J.; Palmer, A. G.; Rance, M.; Skelton, N. *Protein NMR Spectroscopy: Principles and Practice.*; 2nd ed.; Elsevier Academic Press: Burlington, MA, 2007.
(15) James, F.; Roos, M. *Comput. Phys. Commun.* **1975**, *10*, 343-367.
(16) Lipari, G.; Szabo, A. *J. Am. Chem. Soc.* **1982**, *104*, 4546-4559.
(17) Clore, G. M.; Szabo, A.; Bax, A.; Kay, L. E.; Driscoll, P. C.; Gronenborn, A. M. *J. Am. Chem. Soc.* **1990**, *112*, 4989-4991.
(18) Yao, L.; Voegeli, B.; Ying, J. F.; Bax, A. *J. Am. Chem. Soc.* **2008**, *130*, 16518-16520; Yao, L.; Grishaev, A.; Cornilescu, G.; Bax, A. *J. Am. Chem. Soc.*, **2010**, *132*, 4295-4309.